ACS APPLIED MATERIALS & INTERFACES

Research Article

www.acsami.org

Optimizing $LiFePO_4$@C Core–Shell Structures via the 3-Aminophenol–Formaldehyde Polymerization for Improved Battery Performance

Zi-xiang Chi,[†] Wei Zhang,[†] Xu-sheng Wang,[‡] Fu-quan Cheng,[‡] Ji-tao Chen,[‡] An-min Cao,*[,†] and Li-jun Wan*[,†]

[†]Key Laboratory of Molecular Nanostructure and Nanotechnology and Beijing National Laboratory for Molecular Sciences, Institute of Chemistry, Chinese Academy of Sciences (CAS), Beijing 100190, P. R. China

[‡]College of Chemistry and Molecular Engineering, Peking University, Beijing 100871, P. R. China

Supporting Information

ABSTRACT: Polyanion-type cathode materials are well-known for their low electronic conductivity; accordingly, the addition of conductive carbon in the cathode materials becomes an indispensable step for their application in lithium ion batteries. To maximize the contribution of carbon, a core–shell structure with a full coverage of carbon should be favorable due to an improved electronic contact between different particles. Here, we report the formation of a uniform carbon nanoshell on a typical cathode material, $LiFePO_4$, with the shell thickness precisely defined via the 3-aminophenol–formaldehyde polymerization process. In addition to the higher discharge capacity and the improved rate capability as expected from the carbon nanoshell, we identified that the core–shell configuration could lead to a much safer cathode material as revealed by the obviously reduced iron dissolution, much less heat released during the cycling, and better cyclability at high temperature.

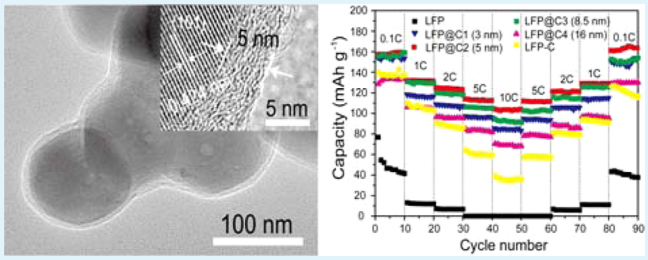

KEYWORDS: *core–shell structure, lithium ion batteries, carbon coating, iron dissolution, cathode materials*

1. INTRODUCTION

For polyanion-type cathode materials $LMPO_4$ (M=Fe, Mn, or Ni), on account of their intrinsic low electronic conductivity and low Li^+ ion diffusion rate, the introduction of conducting carbon has been widely accepted as an inevitable treating process in terms of improving their electrochemical performance.[1−3] As compared to a simple mixture of carbon and $LMPO_4$, a core–shell structured cathode material with a conformal carbon nanoshell is more reasonable choice as far as the conducting effect is considered. A full carbon coverage can encourage an all-dimensional electron conduction between different particles,[4] leading to a reduction of the polarization phenomenon and an improved rate-capability of the cathode materials.[4,5] However, such a surface coating layer could also be an additional barrier, which will impede the lithium ion transportation and then increase the interfacial charge-transfer resistance between electrode and electrolyte.[6,7] Therefore, a systematic optimization on the core–shell configuration becomes necessary so as to achieve a balance between the electronic conductivity and lithium ion diffusion.[7,8] Moreover, to make sure the cathode materials can be ready for their practical applications, simple and easy coating protocols starting from cheap reactants are highly favorable from the economic point of view.

Recently, it has been reported that the formation of resorcinol–formaldehyde (RF) resin would go through a sol–gel process in a way similar to the silica-like Stöber process,[9] resulting in the formation of monodisperse polymer spheres.[10,11] Meanwhile, it is also well-known such a Stöber process can be very successful to form an amorphous silica shell at the presence of different kinds of seeds.[12,13] Therefore, it is becoming a matter of course for researchers to investigate the possibility of forming a polymer coating of RF resin on different substrates.[14−16] Considering the fact that certain phenol derivatives show similar structures to resorcinol, for example, 3-aminophenol (3-AP), it is therefore highly possible that the 3-aminophenol–formaldehyde (3-AF) polymerization can also be a good candidate for the formation of polymer nanoshells.[17] More importantly, the resin polymer possesses a high thermal stability and can be further carbonized into conductive carbon upon high-temperature treatment, which promises a good potential for designing and optimizing the above-mentioned core–shell configuration for $LMPO_4$ cathodes.

In our pursuit of better cathode materials, we paid special attention to the structural stability and the heat released during

Received: October 7, 2014
Accepted: December 2, 2014
Published: December 2, 2014

Scheme 1. Schematic Illustration of the Synthesis of LFP@C Composites and the Coating Mechanism of 3-AF Polymerization

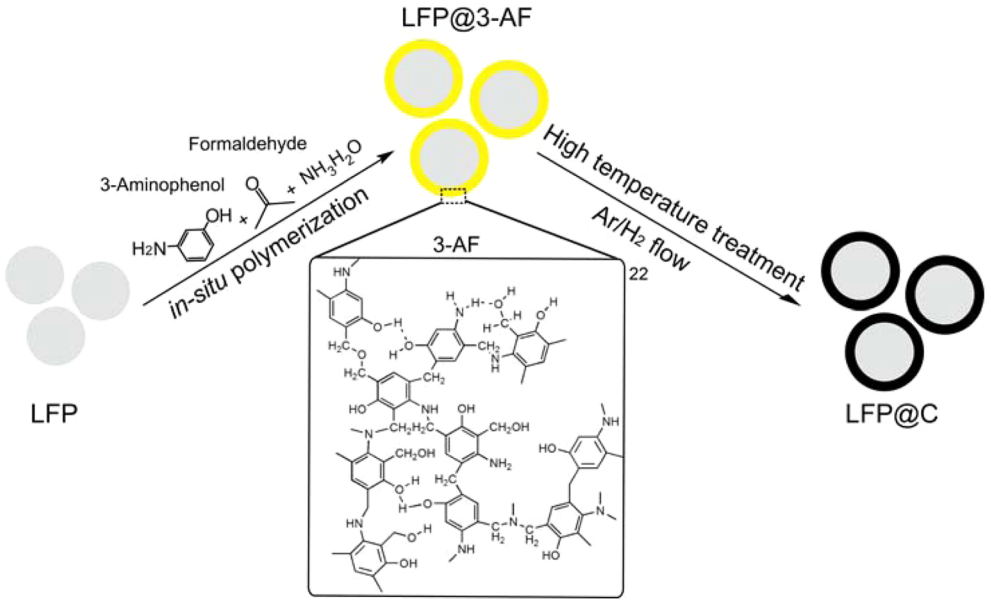

the battery cycling, which are important factors for the practical application of lithium ion batteries as far as the safety issue is concerned. Because of the high energy density of the lithium ion battery system, the interaction between the electrode and electrolyte is inevitable, releasing heat and causing a potential thermal runaway if not managed well.[18] On the other hand, the $LMPO_4$-based cathode materials themselves are prone to suffer from a serious metal dissolution at elevated temperature, resulting in poor thermal stability and thus leading to accelerated capacity fading.[19−21] It has become the task of scientists and engineers to work on broad safety strategies so that the electrical, chemical, and other properties of the electrode materials can be tailored so that a stable system can be created to battle the safety problem. A shield around the electrode materials is reasonably a good choice to alleviate the side reactions and protect the cathode materials.

Herein, we report the formation of uniform carbon nanoshell on $LiFePO_4$ by means of 3-AF polymerization. Typical core−shell structures such as $LiFePO_4$@carbon (LFP@C) with uniform and conformal carbon layer can be easily prepared with the thickness of carbon layer to be precisely defined. Accordingly, the battery performance of the core−shell structured cathode materials could be optimized by means of the systematic control on the surface structure. Detailed investigations revealed that the carbon nanoshells were very effective in improving the battery performance of LFP at a broad range of working temperatures. The existence of a uniform shell around each LFP particle turned out to be a good strategy toward safer cathode materials as revealed by the obviously reduced iron dissolution and much less heat released during the battery cycling.

2. RESULTS AND DISCUSSION

The formation of LFP@C composites is schematically illustrated in Scheme 1. The whole procedure includes two steps. First, 3-AP and formaldehyde will polymerize on the surface of LFP particles to form a thin layer of 3-AF resin under the catalysis of ammonia,[22] forming a typical core−shell structure with LFP as the core and 3-AF resin as the shell (denoted as LFP@3-AF). The surface coated 3-AF resin is then transferred into the conductive carbon (denoted as LFP@C) in the second step by high temperature under a reductive atmosphere.

Figure 1a is the transmission electronic microscopy (TEM) image of the pristine LFP particles. As revealed by the high-resolution TEM (HRTEM) characterization on a randomly selected particle, it is highly crystalline with a clear surface

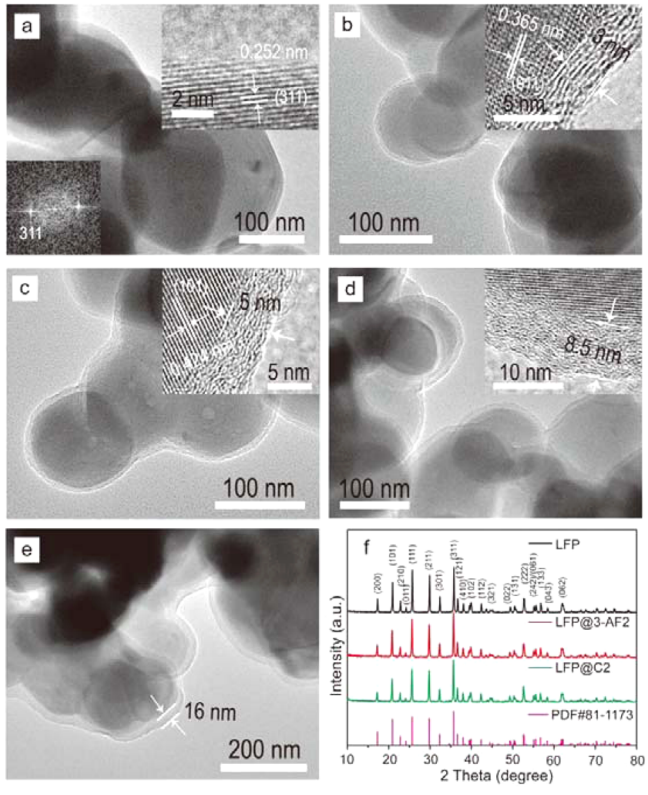

Figure 1. TEM images of pristine LFP (a), LFP@C1 (3 nm coating) (b), LFP@C2 (5 nm coating) (c), LFP@C3 (8.5 nm coating) (d), and LFP@C4 (16 nm coating) (e); (f) XRD patterns of LFP, LFP@3-AF2, and LFP@C2, respectively.

dx.doi.org/10.1021/am506860e | ACS Appl. Mater. Interfaces 2014, 6, 22719−22725

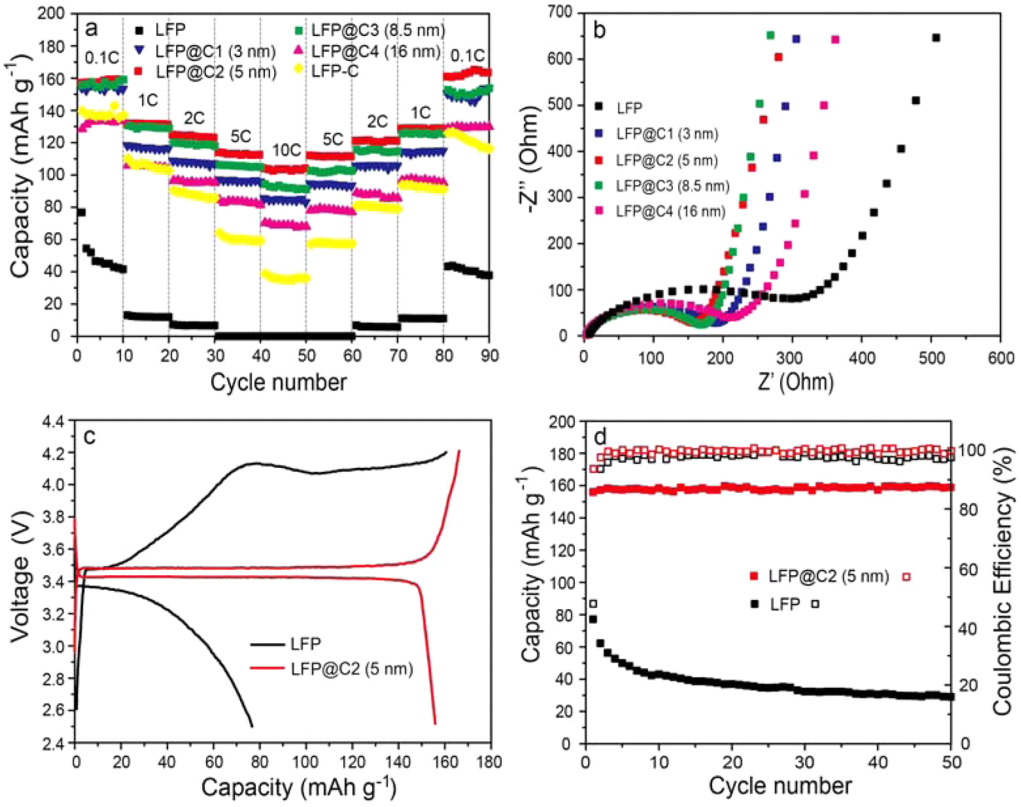

Figure 2. (a) Comparison of the rate-capability among LFP, LFP@C1−4 and LFP-C; (b) EIS spectra for LFP and LFP@C1−C4 with the frequency range of 100 kHz to 100 MHz; (c) first charge/discharge curves of LFP and LFP@C2 at 0.1C; (d) comparison of the cyclability between LFP@C2 and LFP in 50 cycles. (all measured at 25 °C).

borderline (inset, Figure 1a). After the above-mentioned two-step coating treatments, namely, the 3-AF polymerization and its subsequent carbonization process, the particles show observable changes on their surface structures. As shown in Figure 1b, a thin layer emerges on each LFP particle when a high LFP concentration (126.8 mM) and a lower 3-AF concentration (13.1 mM) were used in the polymerization step, forming an obvious core−shell structure (denoted as LFP@C1). The layer is uniformly distributed, and the thickness is measured to be ∼3 nm by HRTEM observation, which is shown in the inset of Figure 1a. Though the carbon layer is very thin, it turns out to be fairly continuous and covers all the LFP nanoparticles. A close observation on the surface carbon shell reveals the existence of irregular lattice fringes of carbon due to the carbonization process.

The core−shell configuration becomes further apparent when the coating shell gets thicker. Our synthesis trials show that the carbon thickness can be easily tuned by simply adjusting the concentrations of the starting materials or the length of the polymerization time. Either an increase in the concentration of 3-aminophenol (3-AP) or a decreased amount of LFP seeds can provide a thicker shell. For example, when we change the concentration of LFP and 3-AP to 56.3 and 14.1 mM, respectively, thicker carbon layer can be achieved as shown in Figure 1c (sample denoted as LFP@C2). HRTEM image confirms the thickness of the surface layer is ca. 5 nm (inset, Figure 1c). Similarly, the carbon shell on LFP can be further controlled to 8.5 nm (shown in Figure 1d, denoted as LFP@C3) and 16 nm (shown in Figure 1e, LFP@C4) (see Experimental Section for details). In fact, we conclude from our synthesis efforts that by fine adjustments of the initial amount of LFP and aminophenol, the thickness of the coating layer can be tuned at a very precise level, even with one-nanometer-accuracy, showing a versatile capability for surface control.

The above thickness-controlled coating shells were fulfilled under the fixed reaction time of 20 h for 3-AF polymerization onto LFP particles. The coating layer can also be modulated by simply varying the polymerization time. For instance, if the 3-AF polymerization was terminated after 1, 3, 6, and 16 h, respectively, in the synthesis of LFP@C4, carbon shells of 2.6, 4, 7, and 13 nm were obtained after carbonization as shown in Supporting Information, Figure S1. This time-based surface-control capability manifests the silica-like sol−gel characteristics in 3-AF polymerization.

For a better understanding of the polymerization process, different characterizations were carried out. For the above-mentioned LFP@C samples, the TEM images of their corresponding precursors as LFP@3-AF are shown in Supporting Information, Figure S2. These LFP@3-AF precursors exhibit the same surface morphology as their carbonized counterparts. They also have obvious core−shell structures but with relatively thicker coating layers on the surface. The 3-AF shells are ∼4, 8, 13, and 20 nm in thickness for LFP@3-AF1−4, thicker than their carbonized counterparts in LFP@C1−4, which is reasonable since the carbonization process will shrink the surface layer as the mass lost during the high-temperature treatment. X-ray diffraction (XRD) (Figure 1f) and SEM (Supporting Information, Figure S3) characterizations on samples of LFP, LFP@3-AF2, and LFP@C2 show that there are no structural or shape changes on the samples before and after the surface treatments. The patterns for all the three samples are almost identical, which can be well-indexed to

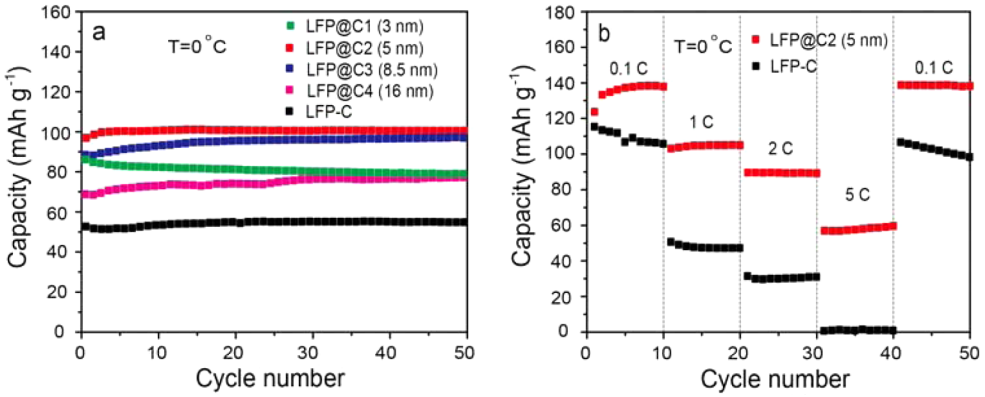

Figure 3. (a) Cyclibility of LFP@C1−C4 at 1 C rate measured at 0 °C. (b) Comparison of rate-capability performance among LFP-C and LFP@C2 at 0 °C.

an orthorhombic space group of LFP powder (JCPDS No. 81−1173).

Meanwhile, Fourier-transform infrared (FT-IR) and Raman spectroscopies were performed to track the surface change during the whole synthesis. Supporting Information, Figure S4a is the comparison of IR patterns among LFP, LFP@C2, LFP@3-AF2, and 3-AF. Specifically, the N−H and O−H stretching vibrations between 3600 and 3100 cm^{-1},[23] the N−H shearing vibration at 1520 cm^{-1},[24] the C═C stretching vibration in the aromatic rings at 1621 and 1438 cm^{-1},[25] and the phenolic C−O−H stretching vibration at 1298 cm^{-1}[24,26] are fingerprint peaks for 3-AF resin, confirming the existence of 3-AF resin in LFP@3-AF. These peaks are not visible in the spectrum of LFP@C2 due to the carbonization process. Raman spectrum of LFP@C2 confirms the emergence of carbon as shown in Supporting Information, Figure S4b. The characteristic peaks at 1593 and 1340 cm^{-1} are Raman fingerprints for the G and D band[27,28] of carbon, respectively, indicating the successful transformation of 3-AF shell into a conductive carbon layer through the high-temperature treatment.

The uniformity of carbon layer for these surface-controlled samples endows us with an ideal model system for systematically evaluating the correlation between the coating effect and the electrochemical performance. Figure 2a gives a comparison of the rate capabilities among these surface-controlled electrodes of LFP@C1−4 at 25 °C. Because of the barren carbon content, the pristine LFP sample shows a discharge capacity of only 62.2 mAh g^{-1} even at a low discharge current of 0.1 C (1 C = 170 mA/g), and a capacity fading is obvious during the first 10 cycles. When it comes to higher rate-currents 1, 2, 5, and 10 C, it is almost unable to discharge any capacities. As expected, the core−shell structured LFP samples, namely, LFP@C1−4, show much improved capacity at different C rates. Among them, the LFP@C2 sample with 5 nm coating layer shows the most obvious advantage. It shows capacities of ∼158, 131, 124, 113, and 105 mAh g^{-1} at 0.1, 1, 2, 5, and 10 C, respectively, exhibiting the optimal performance among all the carbon-coated samples. Although a thicker carbon coating is considered to be beneficial to the electron conduction, an obvious inferiority is identified for the discharge capacities of LFP@C4, which is probably because an overly thick carbon layer would lead to a longer diffusion distance for lithium ion and further increase the interfacial charge-transfer resistance between electrode and electrolyte.[7,29] A 5 nm coating shell probably reflects a good balance between electronic conductivity and Li^+ transport. It is also worth noting that, although the battery performances of core−shell structured LFP@C samples show difference because of the coating thickness of carbon, they are all better than a simple mixture of LFP and carbonized 3-AF (sample denoted as LFP-C) at different C rates, which clearly highlights the advantage of designed core−shell configurations.

To facilitate our understanding of this surface layer-related battery performance, we carried out electrochemical impedance spectroscopy (EIS) on all the LFP@C electrodes. Figure 2b shows the Nyquist plots for different thickness-controlled samples, and LFP@C2 has the smallest radius of the semicircle in the high-to-medium frequency range compared with LFP@C1, C2, and C4. Such a radius indicates the charge transfer and surface film resistance (R_{ct}), which is related to lithium ion interfacial transfer between the electrolyte and the active material.[30] It therefore suggests that the charge transfer and interface reaction occurs easiest for the 5 nm carbon nanoshell, exhibiting the optimal balance between electronic conductivity and Li^+ ionic diffusion, which also explains well its superior rate capability.

Our battery tests also reveal a good cyclic stability of LFP@C2 sample. Figure 2c shows the charge−discharge curves of LFP and LFP@C2 for the first cycle. Compared with pristine LFP, LFP@C2 shows a much improved capacity of 156 mAh g^{-1} for the first cycle, and a much wider platform, which represents the Fe^{3+}/Fe^{2+} redox equilibrium. A few of the following voltage profiles (cycle 10, 20, 30, 40, and 50, for instance) of LFP and LFP@C2 are shown in Supporting Information, Figure S5 for detailed comparison. In the following 50-cycle running shown in Figure 2d, LFP@C2 stably maintains its capacity at ∼159 mAh g^{-1} with no obvious fading, and the Coulombic efficiencies are constant at ∼100%. Supporting Information, Figure S6 shows the TEM image of LFP@C2 after being cycled 90 times. The carbon layer is well-preserved in a continuous and uniform style. No shedding of carbon layer is detectable, and the thickness remains ∼5 nm (HRTEM shown in inset of Supporting Information, Figure S6), indicating the core−shell structured LFP@C is fairly stable during cycling. We believe that such a stable core−shell configuration can provide a good guarantee for the structural stability and the long-term cycling, which is promising for its practical applications in lithium ion batteries.

We also measured the electrochemical performance of the core−shell structured LFP@C samples at a lower temperature environment (0 °C), to make a comprehensive evaluation on the effect of surface carbon. LFP-C was selected as the control

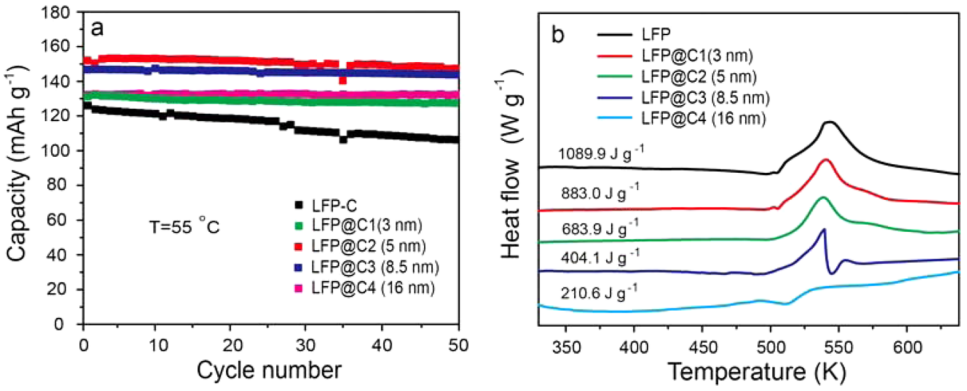

Figure 4. (a) Cyclability of LFPC1-C4 at 1 C rate measured at 55 °C; (b) DSC profiles of pure LFP, LFP@C1, LFP@C2, LFP@C3, and LFP@C4. Charged to 4.2 V.

sample. As shown in Figure 3a, because of a better surface-conducting ability, all the core−shell structured LFP@C samples exhibit much-improved discharge capacities, compared with the mixture of carbonized 3-AF and LFP (LFP-C) sample (~55 mAh g^{-1} at 1 C rate). Among them, LFP@C2 with 5 nm carbon coating shows the best performance of 102 mAh g^{-1}, which is ~80% retention of the capacity at 25 °C. Further rate-capability tests were performed on LFP-C and LFP@C2, as shown in Figure 3b. LFP@C2 can provide the discharge capacities of 138, 105, 90, and 60 mAh g^{-1} at 0.1, 1, 2, and 5 C, respectively, showing a distinct advantage over LFP-C, which confirms the positive role of a conformal carbon coating for LFP at low temperature.

At elevated temperatures, it is reported that polyanion-type cathode materials are subject to the transition metal dissolution, leading to an accelerated capacity fading.[19−21] We find that the core−shell structure can significantly alleviate this problem. A quick cycling running test at 1 C-rate was carried out at 55 °C for different LFP@C samples. As shown in Figure 4a, a mixture of carbon and LFP (LFP-C) suffers a serious capacity fading from 127 to 103 mAh/g after 50 cycles. On the contrary, for core−shell structured LFP@C1−4, the capacity fading has been effectively alleviated as the coating thickness increases. Especially for the LFP@C4 sample (16 nm of coating thickness), it can constantly give a discharge capacity of ~135 mAh g^{-1} with no fading at all. To verify the role of carbon layers in this capacity loss alleviation at elevated temperature, we measured Fe dissolution concentrations in the electrolyte after an extended storage period by ICP-AES (seeing Experimental Section for details). As shown in Table 1, carbon coating layers are proved to be very effective in inhibiting the Fe dissolution, and the dissolved Fe diminishes with the increase of carbon thickness. With the help of 3, 5, 8.5, and 16 nm of carbon coating, the Fe dissolution concentration was greatly reduced from 134 mg/L for pristine LFP to 33.6, 31.1, 18.6, and 10.2 mg/L for LFP@C1−C4, respectively, which well explains the alleviation of capacity loss for LFP@C1−C4 cycling at 1 C rate under 55 °C.

Table 1. Fe Dissolution of LFP, LFP@C1−C4 after Storing for 10 d at 55 °C (1 M $LiPF_6$ in EC/DMC/DEC = 1:1:1)

	pure LFP (no coating)	LFP@C1 (3 nm)	LFP@C2 (5 nm)	LFP@C3 (8.5 nm)	LFP@C4 (16 nm)
Fe dissolution (ppm)	134	33.6	31.1	18.6	10.2

The surface carbon can also effectively inhibit the generated exothermal heat in the battery, which is highly favorable on account of the increasingly strict safety problems faced by the Li-ion battery industry.[31,32] Differential scanning calorimetry (DSC) analysis was carried out on all the LFP materials, which were charged to 4.2 V (see the Experimental Section for details). Figure 4b shows the DSC results recorded in the temperature range of 330−638 K with a heating rate of 10 K min^{-1}. Though there is no obvious difference observed in the starting points of the exothermic heat flow (~510 K), the heat release is much reduced as the carbon shells get thicker. For the pure LFP sample, the total exothermic heat evolution is ~1089.9 J g^{-1}. While it is greatly reduced down to ~883.0, 683.9, 404.1, and 210.6 J g^{-1} when the carbon thickness increased to 3 nm (LFP@C1), 5 nm (LFP@C2), 8.5 nm (LFP@C3) and 16 nm (LFP@C4) respectively. From the above analysis, it can be seen that the conformal carbon shell plays very positive roles in combating the safety problems as revealed by the alleviated Fe dissolution and heat release.

3. EXPERIMENTAL SECTION

Synthesis of LFP Nanoparticles. The pristine $LiFePO_4$ powder was synthesized via solid-state reactions. Source materials including Li_2CO_3, $Fe_2C_2O_4$, and $NH_4H_2PO_4$ are stoichiometrically mixed together (mole ratio of Li/Fe/P = 1.03:1:1). The mixture were milled using a planetary ball mill with ball-to-powder ratio of 4:1 (ball diameter = 10 mm), rotating speed of ~200 rpm, and ball-milling time of 6 h. The product was then collected and subject to high-temperature treatment at 700 °C under a H_2/Ar flow. The collected sample was then used as the pristine LFP sample with a very low carbon content at less than 0.1%.

Synthesis of Thickness-Controlled LFP@C Composites. LFP@C composite with the thickness of ca. 3 nm carbon coating (denoted as LFP@C1) was synthesized as follows: LFP nanopowders were dispersed in a mixed solvent of H_2O and ethanol (H_2O/EtOH = 2:1, v/v) under ultrasonication to make a suspension with the concentration of 126.8 mM. Subsequently, 3-AP was added into the suspension, which was kept stirring to reach a concentration of 13.1 mM. Next, a small amount of ammonia ($NH_3{\cdot}H_2O$, 25%) was added to the mixture to adjust the pH value in the range of 9−10. Finally, a certain amount of formaldehyde solution (37 wt %% in H_2O) was added to make sure the mole ratio between 3-AP and formaldehyde fixed at 1:1.4. The mixture was stirred continuously for ~20 h under room temperature, and the color of the mixture gradually turned from light gray to deep yellow during the stirring period. The yellow precipitates (denoted as LFP@3-AF) were collected by centrifugation,

washed three times with deionized water and once with alcohol, and then dried at 80 °C in an electric oven for 5 h. The resulting sample was heated in a quartz tube to 400 °C at a rate of 3 °C/min in Ar/H_2 (95/5 in volume%) atmosphere, kept at this temperature for 2 h, further heated to 700 °C with a heating rate of 5 °C/min, and kept at this temperature for 15 h. The carbon content in LFP@C1 was determined to be 1.3 wt %.

For the synthesis of LFP@C samples with ca. 5, 8.5, and 16 nm (denoted as LFP@C2, LFP@C3, and LFP@C4, respectively), the concentrations of the reactants were adjusted as follows: 56.3 mM LFP and 14.1 mM 3-AP for LFP@C2, 70.4 mM LFP and 20.2 mM 3-AP for LFP@C3, and 42.3 mM LFP and 20.2 mM 3-AP for LFP@C4. The rest of the reaction conditions were the same as for sample LFP@C1. The carbon content for LFP@C2, LFP@C3, and LFP@C4 are 5.6, 7.5, and 13.7 wt %, respectively.

An LFP-C sample was also synthesized for control experiment to compare the influence of coated-carbon and mixed-carbon on the performance of testing materials. The procedures were as follows: a certain amount of 3-AP and formaldehyde was added to a mixed solvent of H_2O and ethanol (H_2O/EtOH = 2:1 v/v) with the pH value adjusted by ammonia to 9−10, and the mixture was kept stirring for 24 h. The obtained yellow 3-AF polymeric resin precipitates were collected and rinsed with water by centrifugation and then dried at 80 °C. Afterward, 0.5 g (70.6 mM) of LFP was mixed with 0.1 g of 3-AF precipitates totally under the same reaction conditions and heat treatments as LFP@C1, C2, C3, and C4. The carbon content of LFP-C sample was determined to be 5.8 wt %.

Characterization. The size and morphology of the LFP, LFP@3-AF, and LFP@C samples were characterized using a JEOL 6701F scanning electron microscope (SEM) operated at 10 kV. TEM and HRTEM were carried out with a JEOL-2100F transmission electron microscope. X-ray diffraction (XRD) data were collected with a Shimadzu XRD-7000s diffractometer equipped with a Cu Kα radiation (λ = 1.540 56 Å) in the range of 10−80°. Raman spectra were obtained with an NTegra spectra system (NT-MDT). FT-IR spectra were recorded in the range of 4000−400 cm^{-1} with Nicolet iN10 IR microscope (Thermo Fisher Scientific). DSC analysis was performed on a Mettler-Toledo DSC1 STAR^e system. The carbon content of the final products was determined by an LECO CS-344 carbon/sulfur analyzer.

Electrochemical Evaluation. Electrochemical measurements were performed using CR2032 coin cells assembled in an argon-filled glovebox with lithium metal as the counter and reference electrodes. Charge and discharge measurements for the cells were carried out on a Land CT2001A battery test system. Galvanostatic tests of the assembled cells were carried out between 2.5 and 4.2 V. The cathodes were prepared by mixing the active materials, super-P (SP), and poly(vinyl difluoride) (PVDF, Aldrich) at a weight ratio of 80:10:10, pasting on a pure Al foil (99.6%, Goodfellow) and cutting into circular electrodes of 0.64 cm^2 area. Celgard polypropylene membrane was used as a separator. The electrolyte consisted of a solution of 1 M $LiPF_6$ in ethylene carbonate (EC)/dimethyl carbonate (DMC)/diethyl carbonate (DEC) (1:1:1, in wt %) obtained from Guotai-Huarong New Chemical Materials Co., Ltd. Electrochemical impedance spectra (EIS) were performed on an electrochemistry workstation (Princeton PARSTAT 2273).

Transition Metal Dissolution. The Fe dissolution measurement was carried out according to a modified method.[18,19] Typically, 500 mg of LFP was stored in a closed vial containing 5 mL of electrolyte solution under Ar atmosphere, and then the mixtures were moisture-contaminated by 100 ppm of H_2O. The solution was removed after 10 d of storage at 55 °C and then was put on a heating plate to totally evaporate the organic electrolyte. A small amount of HNO_3 was added to the residue to dissolve the metal ion. Then the mixture was filtrated to remove the insolubles, diluted to a certain volume (10 mL) by distilled water, and finally analyzed by ICP (Model: ICPE-9000, Shimadzu Corporation) for the presence of Fe.

4. CONCLUSION

In summary, the 3-AF resin had been successfully applied to the synthesis of core−shell structures as LFP@C. A uniform and conform carbon nanoshell could be accordingly formed with the shell thickness precisely defined. Systematic investigation of the surface-controlled LFP@C samples showed that the performance of LFP was closely related to the surface nanoshells, which could not only improve the rate-capability and cyclabilty of the cathode material at a broad range of tested temperatures but also contributed to tackling the safety issues as revealed by the reduced iron dissolution and alleviated heat release during cycling. Detailed investigations identify that a 5 nm carbon shell (corresponding to LFP@C2) is the optimal coating thickness for LFP. Our results illustrated an effective approach for the surface modification of polyanion-type cathode materials and drew an explicit conclusion on an optimized surface-coating condition for LFP sample.

■ ASSOCIATED CONTENT

Ⓢ Supporting Information

Complementary TEM images, SEM images, voltage profiles, and IR and Raman analyses for the LFP@C samples. This material is available free of charge via the Internet at http://pubs.acs.org.

■ AUTHOR INFORMATION

Corresponding Authors

*E-mail: anmin_cao@iccas.ac.cn. (A.-M.C.)
*E-mail: wanlijun@iccas.ac.cn. (L.-J.W.)

Notes

The authors declare no competing financial interest.

■ ACKNOWLEDGMENTS

This work was supported by the major State Basic Research Program of China (973 Program: 2013CB934000; 863 Program: 2013AA030800), the National Natural Science Foundation of China (Grant No. 21373238), and the Chinese Academy of Sciences.

■ REFERENCES

(1) Oh, S. W.; Myung, S. T.; Oh, S. M.; Oh, K. H.; Amine, K.; Scrosati, B.; Sun, Y. K. Double Carbon Coating of $LiFePO_4$ as High Rate Electrode for Rechargeable Lithium Batteries. *Adv. Mater.* **2010**, *22*, 4842−4845.

(2) Sun, C.; Rajasekhara, S.; Goodenough, J. B.; Zhou, F. Monodisperse Porous $LiFePO_4$ Microspheres for a High Power Li-Ion Battery Cathode. *J. Am. Chem. Soc.* **2011**, *133*, 2132−2135.

(3) Wang, G.; Liu, H.; Liu, J.; Qiao, S.; Lu, G. M.; Munroe, P.; Ahn, H. Mesoporous $LiFePO_4$/C Nanocomposite Cathode Materials for High Power Lithium Ion Batteries with Superior Performance. *Adv. Mater.* **2010**, *22*, 4944−4948.

(4) Wang, Y.; Wang, Y.; Hosono, E.; Wang, K.; Zhou, H. The Design of a $LiFePO_4$/Carbon Nanocomposite with a Core-Shell Structure and its Synthesis by an in Situ Polymerization Restriction Method. *Angew. Chem., Int. Ed.* **2008**, *47*, 7461−7465.

(5) Wang, Y.; He, P.; Zhou, H. Olivine LiFePO4: Development and Future. *Energy Environ. Sci.* **2011**, *4*, 805−817.

(6) Zhu, G.-N.; Wang, C.-X.; Xia, Y.-Y. A Comprehensive Study of Effects of Carbon Coating on $Li_4Ti_5O_{12}$ Anode Material for Lithium-Ion Batteries. *J. Electrochem. Soc.* **2011**, *158*, A102−A109.

(7) Dominko, R.; Bele, M.; Gaberscek, M.; Remskar, M.; Hanzel, D.; Pejovnik, S.; Jamnik, J. Impact of the Carbon Coating Thickness on the Electrochemical Performance of $LiFePO_4$/C Composites. *J. Electrochem. Soc.* **2005**, *152*, A607−A610.

(8) Chi, Z.-X.; Zhang, W.; Cheng, F.-Q.; Chen, J.-T.; Cao, A.-M.; Wan, L.-J. Optimizing the Carbon Coating on $LiFePO_4$ for Improved Battery Performance. *RSC Adv.* **2014**, *4*, 7795−7798.
(9) Stöber, W.; Fink, A.; Bohn, E. Controlled Growth of Monodisperse Silica Spheres in the Micron Size Range. *J. Colloid Interface Sci.* **1968**, *26*, 62−69.
(10) Lu, A. H.; Hao, G. P.; Sun, Q. Can Carbon Spheres be Created through the Stöber Method? *Angew. Chem., Int. Ed.* **2011**, *50*, 9023−9025.
(11) Liu, J.; Qiao, S. Z.; Liu, H.; Chen, J.; Orpe, A.; Zhao, D.; Lu, G. Q. Extension of the Stöber Method to the Preparation of Monodisperse Resorcinol-Formaldehyde Resin Polymer and Carbon Spheres. *Angew. Chem., Int. Ed.* **2011**, *50*, 5947−5951.
(12) Li, W.; Zhao, D. Extension of the Stöber Method to Construct Mesoporous SiO_2 and TiO_2 Shells for Uniform Multifunctional Core-Shell Structures. *Adv. Mater.* **2013**, *25*, 142−149.
(13) Sarshar, Z.; Sun, Z.; Zhao, D.; Kaliaguine, S. Development of Sinter-Resistant Core-Shell $LaMn_xFe_{1-x}O_3$@$mSiO_2$ Oxygen Carriers for Chemical Looping Combustion. *Energy Fuel* **2012**, *26*, 3091−3102.
(14) Fuertes, A. B.; Valle-Vigon, P.; Sevilla, M. One-Step Synthesis of Silica@Resorcinol-Formaldehyde Spheres and Their Application for the Fabrication of Polymer and Carbon Capsules. *Chem. Commun.* **2012**, *48*, 6124−6126.
(15) Fang, X.; Liu, S.; Zang, J.; Xu, C.; Zheng, M. S.; Dong, Q. F.; Sun, D.; Zheng, N. Precisely Controlled Resorcinol-Formaldehyde Resin Coating for Fabricating Core-Shell, Hollow, and Yolk-Shell Carbon Nanostructures. *Nanoscale* **2013**, *5*, 6908−6916.
(16) Li, N.; Zhang, Q.; Liu, J.; Joo, J.; Lee, A.; Gan, Y.; Yin, Y. Sol-Gel Coating of Inorganic Nanostructures with Resorcinol-Formaldehyde Resin. *Chem. Commun.* **2013**, *49*, 5135−5137.
(17) Zhao, J.; Luque, R.; Qi, W.; Lai, J.; Gao, W.; Rehan, M.; Gilani, H. S.; Xu, G. Facile Surfactant-free Synthesis and Characterization of Fe_3O_4@3-Aminophenol-Formaldehyde Core-Shell Magnetic Microspheres. *J. Mater. Chem. A* **2014**; DOI: 10.1039/C4TA03821E.
(18) Joachin, H.; Kaun, T. D.; Zaghib, K.; Prakasha, J. Electrochemical and Thermal Studies of Carbon-Coated $LiFePO_4$ Cathode. *J. Electrochem. Soc.* **2009**, *156*, A401−A406.
(19) Koltypin, M.; Aurbach, D.; Nazar, L.; Ellis, B. On the Stability of $LiFePO_4$ Olivine Cathodes under Various Conditions (Electrolyte Solutions, Temperatures). *Electrochem. Solid-State Lett.* **2007**, *10*, A40−A44.
(20) Wang, J.; Yang, J.; Tang, Y.; Li, R.; Liang, G.; Sham, T.-K.; Sun, X. Surface Aging at Olivine $LiFePO_4$: a Direct Visual Observation of Iron Dissolution and the Protection Role of Nano-Carbon Coating. *J. Mater. Chem. A* **2013**, *1*, 1579−1586.
(21) Iltchev, N.; Chen, Y.; Okada, S.; Yamaki, J.-i. $LiFePO_4$ Storage at Room and Elevated Temperatures. *J. Power Sources* **2003**, *119−121*, 749−754.
(22) Zhao, J.; Niu, W.; Zhang, L.; Cai, H.; Han, M.; Yuan, Y.; Majeed, S.; Anjum, S.; Xu, G. A Template-Free and Surfactant-Free Method for High-Yield Synthesis of Highly Monodisperse 3-Aminophenol-Formaldehyde Resin and Carbon Nano/Microspheres. *Macromolecules* **2013**, *46*, 140−145.
(23) Jiang, J.-H.; Zhu, L.-P.; Li, X.-L.; Xu, Y.-Y.; Zhu, B.-K. Surface Modification of PE Porous Membranes Based on the Strong Adhesion of Polydopamine and Covalent Immobilization of Heparin. *J. Membr. Sci.* **2010**, *364*, 194−202.
(24) Xi, Z.-Y.; Xu, Y.-Y.; Zhu, L.-P.; Wang, Y.; Zhu, B.-K. A facile method of surface modification for hydrophobic polymer membranes based on the adhesive behavior of poly(DOPA) and poly(dopamine). *J. Membr. Sci.* **2009**, *327*, 244−253.
(25) Yang, M.; Ma, J.; Ding, S.; Meng, Z.; Liu, J.; Zhao, T.; Mao, L.; Shi, Y.; Jin, X.; Lu, Y.; Yang, Z. Phenolic Resin and Derived Carbon Hollow Spheres. *Macromol. Chem. Phys.* **2006**, *207*, 1633−1639.
(26) Shareef, B.; Waheed, I.; Jalaot, K. Preparation and Analytical Properties of 4-Hydroxybenzaldehyde, Biuret and Formaldehyde Terpolymer Resin. *Orient. J. Chem.* **2013**, *29*, 1391−1397.
(27) Li, W.; Chen, D.; Li, Z.; Shi, Y.; Wan, Y.; Wang, G.; Jiang, Z.; Zhao, D. Nitrogen-Containing Carbon Spheres with very Large Uniform Mesopores: The Superior Electrode Materials for EDLC in Organic Electrolyte. *Carbon* **2007**, *45*, 1757−1763.
(28) Wu, C. Y.; Cao, G. S.; Yu, H. M.; Xie, J.; Zhao, X. B. In Situ Synthesis of $LiFePO_4$/Carbon Fiber Composite by Chemical Vapor Deposition with Improved Electrochemical Performance. *J. Phys. Chem. C* **2011**, *115*, 23090−23095.
(29) Zhang, X.; Xing, Z.; Wang, L.; Zhu, Y.; Li, Q.; Liang, J.; Yu, Y.; Huang, T.; Tang, K.; Qian, Y.; Shen, X. Synthesis of MnO@C Core-Shell Nanoplates with Controllable Shell Thickness and Their Electrochemical Performance for Lithium-Ion Batteries. *J. Mater. Chem.* **2012**, *22*, 17864−17869.
(30) Qin, Z.; Zhou, X.; Xia, Y.; Tang, C.; Liu, Z. Morphology Controlled Synthesis and Modification of High-Performance $LiMnPO_4$ Cathode Materials for Li-Ion Batteries. *J. Mater. Chem.* **2012**, *22*, 21144−21153.
(31) Cho, Y.-D.; Fey, G. T.-K.; Kao, H.-M. The Effect of Carbon Coating Thickness on the Capacity of $LiFePO_4$/C Composite Cathodes. *J. Power Sources* **2009**, *189*, 256−262.
(32) Yamada, A.; Chung, S. C.; Hinokuma, K. Optimized $LiFePO_4$ for Lithium Battery Cathodes. *J. Electrochem. Soc.* **2001**, *148*, A224−A229.